Determination of gas bubble fractionation rates in the deep ocean by laser Raman spectroscopy

S. N. White*, P. G. Brewer, E. T. Peltzer
Monterey Bay Aquarium Research Institute
Moss Landing, CA 95039-9644

Abstract

A new deep-sea laser Raman spectrometer (DORISS – Deep Ocean Raman In Situ Spectrometer) is used to observe the preferential dissolution of CO_2 into seawater from a 50%-50% CO_2-N_2 gas mixture in a set of experiments that test a proposed method of CO_2 sequestration in the deep ocean. In a first set of experiments performed at 300 m depth, an open-bottomed 1000 cm^3 cube was used to contain the gas mixture; and in a second set of experiments a 2.5 cm^3 funnel was used to hold a bubble of the gas mixture in front of the sampling optic. By observing the changing ratios of the CO_2 and N_2 Raman bands we were able to determine the gas flux and the mass transfer coefficient at 300 m depth and compare them to theoretical calculations for air-sea gas exchange. Although each experiment had a different configuration, comparable results were obtained. As expected, the ratio of CO_2 to N_2 drops off at an exponential rate as CO_2 is preferentially dissolved in seawater. In fitting the data with theoretical gas flux calculations, the boundary layer thickness was determined to be ~42 μm for the gas cube, and ~165 μm for the gas funnel reflecting different boundary layer turbulence. The mass transfer coefficients for CO_2 are $k_L = 2.82$ x 10^{-5} m/s for the gas cube experiment, and $k_L = 7.98$ x 10^{-6} m/s for the gas funnel experiment.

Keywords: Instruments; Carbon Dioxide; Gas Flux; Chemical Sensor

*Corresponding author: Now at: Woods Hole Oceanographic Institution, Woods Hole, MA 02543

1. Introduction

The increasing levels of CO_2 in the atmosphere and its potential for global climate change have led to proposals for sequestering CO_2 in the deep ocean (e.g., Brewer, 2000). For any CO_2 sequestration procedure the cost and complexity of CO_2 capture from the combustion stream dominates the economic equation (U.S. Department of Energy, 1999). Thus, ocean injection of a N_2-CO_2 mixture at relatively shallow depth, combined with piped transfer of the dense CO_2 rich sea water formed to great ocean depth, and release of the excess N_2 gas has been proposed (Saito et al., 2000). The trade off is the increased cost of pressurization of the N_2 gas, and thus the use of an enriched CO_2 stream is preferable. These ocean gas injection schemes rely on a rising bubble stream to provide the surface area required for rapid dissolution. We have developed techniques for direct visual observation of rising bubble (Rehder et al., 2002) and droplet (Brewer et al., 2002b) streams in the ocean.

We have carried out novel experiments to determine *in situ* the dissolution rate of gas mixtures injected into the deep ocean. Our purpose was to test under field conditions a proposal for ocean CO_2 sequestration without prior CO_2 capture (Kajishima et al., 1997; Saito et al., 2000) based upon the marked difference in solubilities of CO_2 (Aya et al., 1997; Haugan and Drange, 1992) and N_2 (Wiebe et al., 1933) gases in cold sea water at high pressure. The dissolution behavior of gas bubbles is of fundamental interest to ocean scientists for reasons as diverse as their role in air-sea gas exchange (Keeling, 1993), to the fate of gases vented from the deep ocean floor (Massoth et al., 1989; Merewether et al., 1985; Rehder et al., 2002). Additionally we sought to advance the use of newly developed Raman spectrometric techniques (Brewer et al., 2004; Pasteris et al., 2004) for deep-sea geochemical studies. Laser Raman spectroscopy is useful for both chemical identification and for observations of the rate of change of gas composition with time.

Raman spectrometry has seen little use as a tool by ocean scientists, but it offers the potential of rapid, non-destructive analysis of solids, liquids, and gases and recent technical developments (Brewer et al., 2004; Pasteris et al., 2004) have enabled its use in the deep sea. The complexity of the typical optical path has in the past rendered Raman most useful as a chemical identification tool rather than for quantitative analysis. However, relative concentrations of gas mixtures can readily be determined by measuring peak area ratios in the spectra, and there exists substantial opportunity for quantitative work where effective calibration protocols are possible (Sum et al., 1997; Wopenka and Pasteris, 1987). Here we take advantage of the rapidity and specificity of the Raman ratio technique and directly observe *in situ* the changing composition of a CO_2-N_2 gas mixture with time during two cruises in August and October of 2002.

2. Methods

2.1. Raman Scattering

Raman scattering is the inelastic, molecular scattering of monochromatic radiation. An incident photon exchanges energy with the target molecule and is scattered with lower or higher energy – Stokes and anti-Stokes scattering, respectively (Figure 1). The observed energy shift of the scattered radiation is equal to the change in vibrational energy of the molecule, and is not dependent on the frequency of the exciting radiation. One of the big advantages of Raman spectroscopy is that it is capable of analyzing solids, liquids, and gases. It is rapid and requires little to no sample preparation, and is (generally) non-destructive. A fuller discussion of the theory behind Raman scattering can be found in Ferraro, et al. (2003), Nakamoto (1997), and references therein.

The intensity of Raman scattering is dependent upon a number of parameters and can be written in simple form as:

$$I_R = (I_L \sigma \eta) P \cdot C \tag{1}$$

where I_R is the measured Raman intensity, I_L is the laser intensity, σ is the Raman cross-section or scattering efficiency, η includes instrument parameters such as optical transmission and collection efficiency, P is the sample path length, and C is the concentration (Pelletier, 1999). The Raman cross-section differs for different molecules and different phases. Additionally, Raman intensity is affected by the optical path; therefore peak heights or areas cannot necessarily be compared directly from one measurement to the next. However, peak ratio techniques, which are independent of optical path, exposure time, and other experimental factors, may be used to determine relative concentrations.

We use the ratio method of Wopenka & Pasteris (1987) in a manner similar to Sum et al. (1997) for a two-component system to obtain an expression relating the concentration C_i of species A and B to the measured Raman band areas (A_i), Raman cross sections (σ_i), and the instrumental factors (η_i) by

$$\frac{C_A}{C_B} = \frac{A_A}{A_B} \frac{\sigma_B}{\sigma_A} \frac{\eta_B}{\eta_A} = \frac{A_A}{A_B} \times \frac{F_B}{F_A} \tag{2}$$

where F_i is defined as the "Raman quantification factor." This yields an expression similar to Beer's Law, widely used in spectrophotometric procedures. In a similar manner, since the fundamental measurement of the molar absorptivities etc. is difficult, Beer's Law is usually applied by constructing a calibration curve. In this case the practical protocols for *in situ* calibration are still evolving, and we use here a single internal reference standard. Sum et al. (1997) have shown that CH_4-CO_2 gas mixtures measured by Raman spectroscopy have a linear calibration curve, and thus although it was not possible to introduce a number of contained known gas mixtures to the probe to provide a direct gas based calibration, we assume that the less complex N_2-CO_2 mixture also yields a linear response.

2.2. *Instrumentation*

Direct measurements of the CO_2-N_2 gas ratio were obtained with MBARI's *in situ* laser Raman spectrometer system called DORISS (Deep Ocean Raman In Situ Spectrometer). This sea-going instrument is based on a laboratory model laser Raman spectrometer (LRS) from Kaiser Optical Systems and consists of a 532 nm Nd:YAG laser, a holographically filtered probe head, a holographic duplex grating, and a 512x2048 front illuminated CCD camera from Andor Technology. The spectral range of DORISS is 100-4400 Δcm^{-1}. The duplex grating splits the spectrum into two stripes on the face of the CCD chip providing a mapping of ~1 cm^{-1} per pixel. The resolution at the time of the deployment was ~7 cm^{-1}.

The instrument is packaged in three pressure housings connected by copper and fiber optic cables for use in the ocean to depths as great as 4000 m (Brewer et al., 2004). The immersion sampling optic used for this experiment has an f/2 lens at the end of a 10 inch-long metal tube with a sapphire window rated to 3000 psi. The working distance of the immersion optic is 4 mm in air, 7 mm in water. The spectrometer was calibrated in the lab prior to deployment. A neon source was used for wavelength calibration and a calibrated tungsten lamp was used for intensity calibration. The laser wavelength was checked by looking at the position of the 801 Δcm^{-1} Raman line of cyclohexane (Tedesco and Davis, 1999). The wavelength calibration of the spectrometer can be affected by changes in temperature (DORISS experienced a temperature drop of ~7°C during the deployment). Therefore, a diamond plate was placed in the beam path of the laser inside the probe head as a reference standard (Brewer et al., 2004; Zheng et al., 2001). The 1332 Δcm^{-1} diamond Raman line is thus superimposed on all collected spectra as a calibration check.

During the time of the deployments discussed here, the instrument was still under development and some components were changed. These components include an X-Y-Z stage (referred to as a laser injector) used to couple the laser to the 62.5 μm excitation fiber. The injector provided by the vendor was replaced by a more robust custom built injector which assured higher laser power output and greater stability. The laser power output was ~11-13 mW for both deployments. Additionally, the slit alignment mechanism in the spectrometer was replaced with a motorized stage. The original slit alignment mechanism was designed to be operated manually with a thumb wheel. Thus, when the spectrometer was sealed in its pressure housing, the slit could not be aligned. Before the motorized stage was installed, no slit was used. Thus the effective slit width was 100 μm (the size of the collection fiber). After the motorized stage was installed, a 50 μm slit was used. Lastly, the diamond chip in the probe head was repositioned between deployments to reduce extraneous scattering off the edges of the chip.

An important characteristic of a new instrument is its detection limit. During the development of the DORISS instrument, changes in configuration have caused changes in sensitivity (and hence detection limit) from one

experiment to another. Additionally, the detection limit is dependent upon the Raman scattering efficiency of the target which varies from one molecule to another. However, based on our August data, we can make some assumptions regarding the detection limit of the instrument. Table 1 shows the signal to noise ratio for the CO_2 and N_2 bands from the August data. The duplex grating used in the spectrometer, divides the spectral region into two stripes – a "high lambda" stripe (~0-2400 Δcm^{-1}) and a "low lambda" stripe (~2200-4400 Δcm^{-1}). The N_2 band is observed on the "high lambda" stripe which has less noise. Assuming that a signal-to-noise ratio of 3 is required, DORISS is capable of detecting concentrations as low as 2.4 mol% for CO_2 and 2.3 mol% for N_2 in this configuration. It should be noted that this is most likely a conservative estimate as improvements to the system which increase sensitivity and decrease noise are currently being implemented.

Table 1

Estimates of DORISS detection limits for gaseous CO_2 and N_2 at 30.86 atm

	Band area (counts)	RMS Noise	Signal-to-Noise	Limit of Detection (S/N = 3)	Limit of Quantification (S/N = 10)
CO_2					
	2917	47	~60	2.4 mol%	8.1 mol%
N_2					
	1965	30	~65	2.3 mol%	7.6 mol%

2.3.   Raman spectra analysis

The spectral data were analyzed using GRAMS/AI data processing software (from ThermoGalactic). Nitrogen has a single Raman peak at 2332 Δcm^{-1}. Carbon dioxide is characterized by the Fermi diad: peaks at ~1285 Δcm^{-1} from the bending mode ($2\nu_2$) and at ~1388 Δcm^{-1} from the symmetric stretch mode (ν_1). The peak position (i.e., Raman shift), height and area were determined using the GRAMS/AI peak fitting routine. When identifying peaks, the same wavenumber regions were analyzed for all spectra, and baseline values were determined by the peak fitting routine for those regions. As noted above, we examined ratios of the CO_2 to N_2 peak areas which are independent of exposure time, optical path, and instrument configuration.

3. Field Experiments

DORISS was deployed in Monterey Bay using MBARI's remotely operated vehicle (ROV) Ventana (Figure 2). The ROV Ventana provides power and communications to DORISS, and is controlled by pilots and scientists aboard the support ship, the R/V Point Lobos, through a ~2 km-long tether. Measurements of the gas mixture were made at depths of 100-400 m (well above the seafloor at

that location). The ROV's external HID lights were turned off during acquisition of spectra. These lights produce strong peaks across the spectral region of the DORISS instrument.

This paper will focus on data collected at 300 m during two dive series. The ambient seawater temperature at that depth was 7.9°C, and the pressure was ~300 dbar. At this temperature and pressure pure CO_2 is a gas and is clearly outside of the hydrate stability field (Figure 3a). However, for this experiment we used a 50-50 (mole %) mixture of CO_2 and nitrogen; for this mixture the phase boundaries are dramatically shifted due to CO_2-N_2 interactions. A liquid phase will not form under any PT conditions encountered in Monterey Bay, nor will CO_2 clathrate hydrate form under the conditions of the experiment (Figure 3b); we calculated the physical properties using MultiFlash 3.2 (Infochem, Inc., London).

A 50-50 (mole %) mixture of carbon dioxide and nitrogen was prepared by first filling an evacuated SCUBA tank to 800 psia with commercial grade CO_2 at ambient temperature (21.9°C) and then filling with UHP nitrogen gas to 1600 psia. This second step was done in two parts by allowing the cylinder to cool to ambient temperature overnight between fillings. We estimate that the composition is within ± 5% of the target mixture based upon uncertainties in the pressure and temperature at time of filling. The SCUBA tank was allowed to sit to achieve complete mixing of the gases for 40 hours before use. The same gas mixture was used for both the August and October deployments.

3.1.   August 2002 experiments

A preliminary set of measurements was obtained in August 2002. During this experiment, the immersion optic was inserted into a hole in the side of an open-bottomed 1000 cm^3 cube; thus the optic tip was in a pocket of gas and no seawater was in the beam path (Figure 4). The gas cube was filled with a 50%-50% CO_2-N_2 gas mixture from a port at the top of the box; thus, very little mixing with seawater occurred during filling. A second valve allowed the box to vent gas upwards while filling with seawater through the open bottom. With this configuration we were easily able to collect quality spectra of a 50%-50% mixture of CO_2 and N_2 gas and 100% N_2 gas. Two sets of measurements where collected at 300 m depth – a series of 10 x 10 sec accumulations spanning 23 minutes, and a series of 5 x 5 sec accumulations spanning 16 minutes. The box was purged and refilled with gas before each experiment.

The gas cube experiment provided a baseline to understand the relative intensities of the Raman signals from CO_2 and N_2. We were also able to observe the preferential dissolution of CO_2 into seawater. However, due to the low ratio of the seawater-exposed area to the gas volume (~0.1 cm^{-1}) we were not able to observe the complete diffusion of CO_2 from the gas cube during the time of our experiment (~30 minutes).

3.2.   October 2002 experiments

In October of 2002 we performed another series of experiments to observe the preferential dissolution of CO_2 from a 50%-50% CO_2-N_2 gas mixture. Based upon the results from our August cruise we were able to scale the experiment appropriately, such that complete CO_2 dissolution could be observed in ~30 minutes. The probe head was positioned in a downward-looking orientation and a clear conical funnel was placed on the tip of the immersion optic to hold a buoyant gas bubble in the DORISS beam path (Figure 5). The total volume of the funnel was 2.5 cm^3, and the ratio of the exposed area to the gas volume was increased 20-fold from the earlier gas cube experiment.

Two experiments were run with the funnel configuration, both at a depth of 300 m, with spectra being collected every 5 minutes over a 30 minute period. During the first run, each spectrum was an average of 10 accumulations of 10 second exposures. Thus, each spectrum was an average over a time span of 100 seconds. During the second run, each spectrum was an average of fifteen 15-second exposures (time span of 225 seconds). The funnel was thoroughly flushed with the gas mixture prior to each experiment.

4. Results

4.1.   August 2002 data

The data from the August dives provide information on the relative Raman scattering efficiencies of nitrogen and carbon dioxide. Initial spectra from both experiments are shown in Figure 6. The two CO_2 peaks (~1285 and ~1388 Δcm^{-1}) are separated by the diamond reference peak (1332 Δcm^{-1}) in the left half of the spectrum; the N_2 peak (2332 Δcm^{-1}) is on the right half of the spectrum. The dropout at 1942 Δcm^{-1} is due to a flaw on the CCD chip. We compared the area ratios of both CO_2 bands to the N_2 band to examine any differences in the Raman efficiencies. Immediately after the cube was filled, the ratio of the CO_2 bend band (~1285 Δcm^{-1}) to N_2 was ~1.1; the ratio of the CO_2 stretch band (~1388 Δcm^{-1}) to N_2 was ~1.9. These ratios were the same for both sets of measurements – 10 x 10 sec exposures and 5 x 5 sec exposures. The peak area ratios observed over time (Figure 7) show the decrease in CO_2 relative to N_2 in the gas mixture. The 5 x 5 sec accumulations show more scatter in the data than the 10 x 10 sec accumulations as expected due to higher noise levels in shorter exposures.

4.2.   October 2002 data

The data from the October dives provide information on the rate at which CO_2 is preferentially dissolved into seawater. Two sets of measurements were made with the small funnel configuration (Figure 5) – a series of 10 x 10 sec accumulations and a series of 15 x 15 sec accumulations each spanning ~30 minutes. It should be noted that in the raw data the diamond peak area is

approximately the same in the October data as it is in the August data. However, the peak areas of the gas components are ~2.5 times as strong in the August data as they are in the October data. This is due to the changes in the instrument between cruises and differences in the optical path for the two experiments (i.e., the large gas cube used in August versus the small gas funnel used in October). Despite the fact that the absolute peak area values are different, the peak area ratios are not affected and can be compared.

The October data show starting ratios of ~1.5 for the CO_2 stretch band to N_2, and ~0.8 for the CO_2 bend band to N_2. These numbers are slightly lower than those observed from the August dives (~1.9 and ~1.1, respectively). This is likely due to the fact that a) the gas is bubbled up into the funnel through seawater allowing some gas dissolution, and b) the scaling of the experiment leads to faster dissolution of CO_2 as compared to the gas cube experiment. Thus, some CO_2 dissolution has already occurred before (or while) the initial spectra are being obtained. Calculations and comparisons with the August data suggest that the starting ratio for the October experiments is actually ~44%-56% CO_2-N_2.

During the October experiments, the complete dissolution of CO_2 can be observed within ~30 minutes. Spectra were collected every five minutes during this time and show the decreasing CO_2 Raman peaks (Figure 8). The CO_2 peaks were much smaller in the October measurements than they were in the August measurements (Figure 6) with respect to the diamond peak. By plotting the ratios over time we can fit an exponential curve to the data (Figure 9, Table 2). The exponential drop off of the data is due to the fact that since CO_2 is preferentially dissolved, the mole fraction of CO_2 in the gas mixture decreases over time which leads to a slowing of the dissolution rate.

Table 2

Curve Fits for October 2002 data

Area Ratios	Least Squares Fit	r^2
Experiment 1 – 10 x 10 sec		
CO_2 stretch / N_2	$1.60\ e^{-0.0587\ x}$	0.989
CO_2 bend / N_2	$0.865\ e^{-0.0583\ x}$	0.970
Experiment 2 – 15 x 15 sec		
CO_2 stretch / N_2	$1.44\ e^{-0.0536\ x}$	0.947
CO_2 bend / N_2	$0.724\ e^{-0.0532\ x}$	0.904

5. Discussion

5.1.   *Air-sea gas exchange*

The mechanism of gas exchange across an air-water interface has been studied for years in order to better understand ocean interaction with the overlying atmosphere which has implications for global climate. Researchers typically use two-layer models where thin boundary layers are present in both the gas phase and the liquid phase (e.g., Liss and Slater, 1974), or single-layer stagnant boundary layer models where a gradient exists only in the water layer (e.g., Broecker and Peng, 1974). These models assume that both the air and water layers are well mixed while gradients exist only in thin films at the interface.

Our gas dissolution experiments provide a small-scale look at gas transfer across a gas-liquid interface at high pressure, and absent turbulent wind forcing of either the gas or water components; only local ocean water velocities perturb the interface. We assume that both the gas volume and the seawater below it are well mixed, however we do not have knowledge of the diffusive boundary layer thickness. Our initially 50%-50% CO_2-N_2 gas mixture changes composition with time and decreases in total volume as gas is transferred to the seawater below. We will use typical values for the stagnant boundary layer model to calculate expected fluxes and concentrations and compare them to the data collected with the DORISS system.

The gas exchange rate of CO_2 presents a special case due to the complex chemistry involved (Zeebe and Wolf-Gladrow, 2001). Typically it is the much slower rate of atmosphere-ocean CO_2 gas exchange that engages the attention of ocean chemists. Bolin (1960) first drew attention to this, and the phenomenon is due to the buffer capacity of seawater and the relatively long time scales to achieve chemical equilibrium in the oceanic mixed layer within the aqueous CO_2 system.   The net result is a gas exchange rate for CO_2 $\cong$10x slower than for typical atmospheric gases, including nitrogen. However, the approximately 10x greater solubility of CO_2 in seawater (Aya et al., 1997; Haugan and Drange, 1992; Rehder et al., 2004) until the hydrate phase boundary is reached, results in far faster dissolution rates.

5.2.   *Theoretical calculations*

Since we may neglect the complexities of the ocean-atmosphere boundary layer, we may use a simple rendition of the gas exchange equation. From Henry's Law the amount of gas dissolved in a volume of solvent (C_l) is proportional to the partial pressure of the gas (P_g) in the gas volume (atm) in equilibrium with the solution, and the ratio can be described by a solubility constant, K (mol/L/atm).

$$C_l = K \cdot P_g \tag{3}$$

Using the stagnant film model (Broecker and Peng, 1974; Broecker and Peng, 1982), the flux of gas across the interface can be calculated by

$$F = D \cdot \frac{C_{top} - C_{bottom}}{z} \cdot \frac{1}{1000} \qquad (4)$$

where F is the gas flux (mol/cm^2/s), D is the coefficient of molecular diffusion (cm^2/s), C_{top} and C_{bottom} are the concentrations at the top and the bottom of the boundary layer (mol/L), and z is the thickness of the boundary layer (cm). The bottom of the boundary layer is in equilibrium with the seawater below (C_{sw}) and the top of the boundary layer is in equilibrium with the gas layer above (Equation 3). Therefore, Equation 4 can be rewritten as

$$F = D \cdot \frac{K \cdot P_g - C_{sw}}{z} \qquad (5)$$

Values for the equilibrium concentration in seawater, diffusion coefficient, and solubility of CO_2 and N_2 are given in Table 3a for the surface ocean at 1 atm and in Table 3b for a depth of 300 m and 30.86 atm pressure. Literature values for the boundary layer thickness obtained from laboratory experiments vary from ~10 to ~300 μm, while radiocarbon calculations suggest an average ocean boundary layer thickness of ~40 μm (Broecker and Peng, 1974).

At the beginning of the experiment, the partial pressures of CO_2 and N_2 in the gas volume are the same (15.43 atm). The values for the equilibrium concentration in seawater, diffusion coefficient, and solubility of CO_2 and N_2 at 300 m depth are given in Table 3b. Equation 3 shows that for both CO_2 and N_2, the dissolved gas concentration in equilibrium with the gas phase is higher than the gas concentration in seawater. Therefore, both gases should dissolve into seawater over time. Using Equation 5 and assuming a boundary layer thickness of 40 μm, we find that the flux of CO_2 into seawater (1.27×10^{-6} mol/cm^2/s) is much higher than that of N_2 (4.45×10^{-8} mol/cm^2/s) due to its higher solubility. Therefore, the concentration of N_2 in the gas phase should increase over time as CO_2 is preferentially dissolved.

Table 3a

Gas properties for CO_2 and N_2 in the surface ocean (1 atm)

	CO_2	N_2
Gas concentration in seawater, C_{sw} (mol/L) @ 0°C [a]	2.00×10^{-5}	6.20×10^{-4}
Diffusion coefficient, D (cm^2/s) @ 8°C [b]	1.17×10^{-5}	1.21×10^{-5}
Solubility, K (mol/L/atm) @ 8°C [c]	4.72×10^{-2}	6.46×10^{-4}

[a] From Broecker & Peng (1982).
[b] Broecker & Peng (1974), Jähne et al. (1987)
[c] From Weiss (1974), Weiss (1970).

Table 3b

Gas properties for CO_2 and N_2 at 300 m depth (30.86 atm)

	CO_2	N_2
Gas concentration in seawater, C_{sw} (mol/kg) @ 8°C [a,b]	4.90×10^{-5}	5.36×10^{-4}
Diffusion coefficient, D (cm^2/s) @ 8°C [c]	1.17×10^{-5}	1.21×10^{-5}
Solubility, K (mol/L/atm) @ 8°C [d]	2.80×10^{-2}	9.89×10^{-4}

[a]   From CO2sys version 01.05 (Lewis, BNL).
[b]   From Weiss (1970).
[c]   Broecker & Peng (1974), Jähne et al. (1987); Note that diffusion coefficient is not significantly affected by pressure.
[d]   Calculated using MultiFlash 3.2 (Infochem Inc., London).

5.3.   Comparison with Raman measurements

From Equation 2, we see that the area ratio of the CO_2 and N_2 Raman bands is proportional to the ratio of their concentrations. We know the initial concentration of the gases in the gas mixture, which provides us with a calibration point. We can then determine the concentration ratio of the gas mixture over time from the ratio of the Raman peak areas. The mole fractions are determined from the concentration ratios over time and can be compared to theoretical calculations based on the gas flux equation (Equation 5) above.

We first looked at the 10 x 10 sec data from the August 2002 experiment using the 1000 cm^3 gas cube. The cube shape maintains a constant exposed surface area (100 cm^2) as the gas volume decreases. The signal-to-noise ratio of the instrument appears to have been higher by a factor of 5 during this deployment compared to the October deployment. Additionally, the slow rate of dissolution is a good match for the long exposure times (i.e., 10 x 10 sec accumulations, 100 sec total exposure time). The observed data is shown in Table 4. The peak areas of the CO_2 bands (stretching band: ~1388 Δcm^{-1}; bending band: ~1285 Δcm^{-1}) decrease over time corresponding to a decrease in mole fraction and concentration. The peak area of the N_2 peak (~2332 Δcm^{-1}) increases over time, corresponding to an increase in mole fraction and concentration. Concentration ratios are calculated from the ratios of both CO_2 bands to nitrogen. As expected, the concentration ratios determined from each CO_2 band are quite similar. The mean value of the concentration ratio is used to determine the mole fractions of CO_2 and N_2. The density of the gas mixture is calculated using MultiFlash 3.2 from the mole fractions.

Table 5 shows calculated values for moles, mole fraction, partial pressure and gas flux over time. This data is based on the initial conditions (shown in the first row of Table 4) and flux calculations discussed in the previous section. A boundary layer thickness (z) of ~42 µm is needed to approximate the observed

data. As expected the gas flux of CO_2 is much higher than that of N_2 (by a factor of almost 30). As the CO_2 is preferentially dissolved into seawater its mole fraction and flux decrease over time. This slowing of the flux causes the observed exponential drop-off of the data (Figure 9). Based on the calculations, the change in volume of the gas over 1200 sec is 89.88 cm^3. By looking at video frame grabs of the experiment, we observed that the gas volume has decreased by approximately 1 cm in height which is ~100 cm^3 in volume.

The same observational to theoretical comparison can be made for the October data from the 2.5 cm^3 gas funnel. Due to the shape of the funnel, the surface area exposed to seawater decreases over time as the gas volume decreases. Table 6 shows the observed data from the 10x10 second experiments. As noted in section 4.3, the starting gas mixture appears to be 44%-56% CO_2-N_2. The calculated values of moles, mole fraction, partial pressure, and gas flux are shown in Table 7. Unlike the calculations for the August data, a boundary layer thickness of ~165 μm is necessary to approximate the data from the October experiment, possibly due to reduced boundary layer turbulence within the small gas funnel. The rate of change in gas composition in the October experiment is also higher (by as much as an order of magnitude) than those in the August experiment. This is due to the higher seawater-exposed area to gas volume ratio as noted in section 3.2.

A comparison of the observed and theoretical data from the August and October experiments is shown in Figure 10. Due to the volume/exposed surface area scaling of the experiment, the proportion of CO_2 loss occurs more rapidly in the October experiment. In both cases, the theoretical calculations match quite well to the observed data. The August data shows a slight curvature that is not matched by the theoretical line. This may be due to the fact that as the gas volume in the cube decreases an enriched liquid layer is confined in the lower portion of the cube which slows the dissolution rate over time.

Table 4

Observation of CO_2 and N_2 dissolution from the 1000 cm³ gas cube (August 2002, 10x10 sec data)

Elapsed Time	Observed Peak Area (counts)			Observed Concentration Ratios		Mean Conc. Ratio	Mean Observed Mole Fraction		Mean Density
(minutes)	CO_2-bend	CO_2-stretch	N_2	CO_2-bend / N_2	CO_2-stretch / N_2	CO_2/N_2	CO_2	N_2	(g/cm3)
2.835	6570	11510	5970	1.0000	1.0000	1.0000	0.5000	0.5000	0.05247
7.835	6244	10619	6217	0.9127	0.8859	0.8993	0.4735	0.5265	0.05156
12.835	6413	11028	6651	0.8763	0.8601	0.8682	0.4647	0.5353	0.05127
17.835	6355	10961	6888	0.8383	0.8254	0.8319	0.4541	0.5459	0.05091
22.835	6152	10294	6714	0.8326	0.7953	0.8140	0.4487	0.5513	0.05074

Table 5

Theoretical calculation for the 1000 cm³ gas cube

Elapsed Time	Calculated Moles in Gas Cube (moles)			Calculated Mole Fractions		Calculated Partial Pressure (atm)		Calculated Gas Flux (mol/cm²/sec)	
(minutes)	CO_2	N_2	Total	CO_2	N_2	CO_2	N_2	CO_2	N_2
2.835	0.7252	0.7252	1.4505	0.5000	0.5000	15.43	15.43	1.22E-06	4.29E-08
7.835	0.6890	0.7239	1.4130	0.4876	0.5124	15.05	15.81	1.19E-06	4.40E-08
12.835	0.6537	0.7226	1.3763	0.4750	0.5250	14.66	16.20	1.16E-06	4.52E-08
17.835	0.6193	0.7212	1.3406	0.4620	0.5380	14.26	16.60	1.13E-06	4.63E-08
22.835	0.5859	0.7198	1.3058	0.4487	0.5513	13.85	17.01	1.09E-06	4.75E-08

Table 6

Observation of CO_2 and N_2 dissolution from the 2.5 cm^3 gas funnel (October 2002, 10x10 sec data)

Elapsed Time	Observed Peak Area (counts)			Observed Concentration Ratios		Mean Conc. Ratio	Mean Observed Mole Fraction		Mean Density
(minutes)	CO_2-bend	CO_2-stretch	N_2	CO_2-bend / N_2	CO_2-stretch / N_2	CO_2/N_2	CO_2	N_2	(g/cm3)
0.835	1470	2917	1966	0.6795	1.0000	0.8398	0.4565	0.5435	0.05099
5.835	1382	2330	1965	0.6392	0.6150	0.6271	0.3854	0.6146	0.04870
10.835	1033	2007	2092	0.4488	0.4978	0.4733	0.3213	0.6787	0.04672
15.835	925	1498	2279	0.3687	0.3411	0.3549	0.2619	0.7381	0.04497
20.835	602	1258	2394	0.2286	0.2726	0.2506	0.2004	0.7996	0.04321
25.835	578	998	2561	0.2052	0.2022	0.2037	0.1692	0.8308	0.04234
31.665	321	602	2547	0.1146	0.1225	0.1186	0.1060	0.8940	0.04062

Table 7

Theoretical calculation for the 2.5 cm^3 gas funnel

Elapsed Time	Calculated Moles in Gas Cube (moles)			Calculated Mole Fractions		Calculated Partial Pressure (atm)		Calculated Gas Flux (mol/cm^2/sec)	
(minutes)	CO$_2$	N$_2$	Total	CO$_2$	N$_2$	CO$_2$	N$_2$	CO$_2$	N$_2$
0.835	0.001648	0.001962	0.003610	0.4565	0.5435	14.09	16.77	3.15E-07	1.32E-08
5.835	0.001242	0.001943	0.003185	0.3899	0.6101	12.03	18.83	2.69E-07	1.49E-08
10.835	0.000918	0.001923	0.002841	0.3231	0.6769	9.97	20.89	2.23E-07	1.66E-08
15.835	0.000666	0.001902	0.002568	0.2594	0.7406	8.01	22.85	1.79E-07	1.82E-08
20.835	0.000475	0.001880	0.002355	0.2017	0.7983	6.23	24.63	1.39E-07	1.97E-08
25.835	0.000333	0.001857	0.002190	0.1522	0.8478	4.70	26.16	1.05E-07	2.09E-08
31.665	0.000217	0.001830	0.002046	0.1060	0.8940	3.27	27.59	7.31E-08	2.21E-08

6. Conclusions

Saito et al. (2000) have proposed a method for CO_2 sequestration that employs a gas-lift pump (GLAD – Gas Lift Advanced Dissolution) system and would be effective for low-purity CO_2. From laboratory experiments at atmospheric pressure, they have determined the mass transfer coefficients (k_L) for pure CO_2 and a mix of 95% CO_2 and 5% air (Saito et al., 1999). The average mass transfer coefficient for CO_2 is 2.0×10^{-4} m/s, and that of the low purity CO_2 is slightly less. Our work performed at a depth of 300 m (the depth proposed for gas injection in the GLAD system) using a 50%-50% CO_2-N_2 mixture shows a lower CO_2 mass transfer coefficient: $k_L = 7.98 \times 10^{-6}$ m/s for the gas funnel experiment. Saito (1999) showed that the mass transfer coefficient is lower for lower purity CO_2, and this is supported by our lower numbers for a 50% CO_2 gas mixture.

Laser Raman spectroscopy is a useful and valuable tool for performing *in situ* analysis in the deep ocean. Changing processes can be observed in real-time, and both qualitative and quantitative data can be obtained. The novel *in situ* spectroscopic techniques we have devised will enhance many CO_2 and gas hydrate studies (e.g., Brewer et al., 2002a; Brewer et al., 2002b; Rehder et al., 2002; Rehder et al., 2004), and can be extended to a very wide range of ocean science, including hydrothermal vent studies.

References

Aya, I., Yamane, K. and Nariai, H., 1997. Solubility of CO_2 and density of CO_2 hydrate at 30 MPa. Energy, 22(2/3): 263-271.

Bolin, B., 1960. On the exchange of carbon dioxide between the atmosphere and the sea. Tellus, 12: 274-281.

Brewer, P.G., 2000. Contemplating action: Storing carbon dioxide in the ocean. Oceanogr., 13(2): 84-92.

Brewer, P.G., Malby, G.E., Pasteris, J.D., White, S.N., Peltzer, E.T., Wopenka, B., Freeman, J. and Brown, M.O., 2004. Development of a laser Raman spectrometer for deep-ocean science. Deep-Sea Res., 51: DOI:10.1016/j.dsr.2003.11.005.

Brewer, P.G., Paull, C., Peltzer, E.T., Ussler, W., Rehder, G. and Friederich, G., 2002a. Measurements of the fate of gas hydrates during transit through the ocean water column. Geophys. Res. Lett., 29(22): 10.1029/2002GL014727.

Brewer, P.G., Peltzer, E.T., Friederich, G. and Rehder, G., 2002b. Experimental determination of the fate of rising CO2 droplets in seawater. Environ. Sci. Technol., 36: 5441-5446.

Broecker, W.S. and Peng, T.-H., 1974. Gas exchange rates between air and sea. Tellus, 26: 21-35.

Broecker, W.S. and Peng, T.-H., 1982. Tracers in the Sea. Lamont-Doherty Geological Observatory, Palisades, NY, 690 pp.

Ferraro, J.R., Nakamoto, K. and Brown, C.W., 2003. Introductory Raman Spectroscopy. Academic Press, San Diego, CA.

Haugan, P.M. and Drange, H., 1992. Sequestration of CO_2 in the deep ocean by shallow injection. Nature, 357(6376): 318-320.

Jähne, B., Heinz, G. and Dietrich, W., 1987. Measurement of the diffusion coefficients of sparingly soluble gases in water. J. Geophys. Res., 92(C10): 10,767-10,776.

Kajishima, T., Saito, T., Nagaosa, R. and Kosugi, S., 1997. GLAD: A gas-lift method for CO_2 disposal into the ocean. Energy, 22(2/3): 257-262.

Keeling, R.F., 1993. On the role of large bubbles in air-sea gas exchange and supersaturation in the ocean. J. Mar. Res., 51(2): 237-271.

Liss, P.S. and Slater, P.G., 1974. Flux of gases across the air-sea interface. Nature, 247: 181-184.

Massoth, G.J., Butterfield, D., Lupton, J., McDuff, R.E., Lilley, M.D. and Jonasson, I.R., 1989. Submarine venting of phase-separated hydrothermal fluids at Axial Volcano, Juan de Fuca Ridge. Nature, 340: 702-705.

Merewether, R., Olsson, M.S. and Lonsdate, P., 1985. Acoustically detected hydrocarbon plumes rising from 2-km depths in Guaymas Basin, Gulf of California. J. Geophys. Res., 90(4): 3075-3085.

Nakamoto, K., 1997. Infrared and Raman Spectra of Inorganic and Coordination Compounds: Part A. John Wiley & Sons, Inc., New York, NY, 387 pp.

Pasteris, J.D., Wopenka, B., Freeman, J.J., Brewer, P.G., White, S.N., Peltzer, E.T. and Malby, G.E., 2004. Raman spectroscopy in the deep ocean: successes and challenges. Appl. Spec., 58(7): 195A-208A.

Pelletier, M.J. (Editor), 1999. Analytical Applications of Raman Spectroscopy. Blackwell Science Ltd., Oxford, 478 pp.

Rehder, G., Brewer, P.G., Peltzer, E.T. and Friederich, G., 2002. Enhanced lifetime of methane bubble streams within the deep ocean. Geophys. Res. Lett., 29(15): 10.1029/2001GL013966.

Rehder, G., Kirby, S.H., Durham, W., Stern, L., Peltzer, E.T., Pinkston, J. and Brewer, P.G., 2004. Dissolution rates of pure methane hydrate and carbon-dioxide hydrate in undersaturated seawater at 1000 m depth. Geochim. Cosmochim. Acta, 68: 285-292.

Saito, T., Kajishima, T. and Nagaosa, R., 2000. CO_2 sequestration at sea by gas-lift system of shallow injection and deep releasing. Environ. Sci. Technol., 34(19): 4140-4145.

Saito, T., Kajishima, T., Tsuchiya, K. and Kosugi, S., 1999. Mass transfer and structure of bubbly flows in a system of CO_2 disposal into the ocean by gas-lift column. Chem. Eng. Sci., 54: 4945-4951.

Sum, A.K., Burruss, R.C. and Sloan, E.D., 1997. Measurement of clathrate hydrates via Raman spectroscopy. J. Phys. Chem. B, 101: 7371-7377.

Tedesco, J.M. and Davis, K.L., 1999. Calibration of dispersive Raman process analyzers. Proc. SPIE, 3537: 200-212.

U.S. Department of Energy, 1999. Carbon Sequestration Research and Development, Oak Ridge National Lab.

Weiss, R.F., 1970. The solubility of nitrogen, oxygen and argon in water and seawater. Deep Sea Res., 17: 721-735.

Weiss, R.F., 1974. Carbon dioxide in water and seawater: the solubility of a non-ideal gas. Mar. Chem., 2: 203-215.

Wiebe, R., Gady, V.L. and Heins, C., 1933. The solubility of nitrogen in water at 50, 75, and 100 deg from 25 to 1000 atmospheres. J. Am. Chem. Soc., 55: 947-953.

Wopenka, B. and Pasteris, J.D., 1987. Raman intensities and detection limits of geochemically relevant gas mixtures for a laser Raman microprobe. Anal. Chem., 59: 2165-2170.

Zeebe, R. and Wolf-Gladrow, D., 2001. CO_2 in Seawater: Equilibrium, Kinetics, Isotopes. Elsevier, 346 pp.

Zheng, X., Fu, W., Albin, S., Wise, K.L., Javey, A. and Cooper, J.B., 2001. Self-referencing Raman probes for quantitative analysis. Appl. Spectrosc., 55(4): 382-388.

Figures

Figure 1. Raman scattering is the inelastic scattering of monochromatic radiation. An incident photon exchanges energy with the target molecule and is scattered with lower energy (Stokes scattering) than the incident energy.
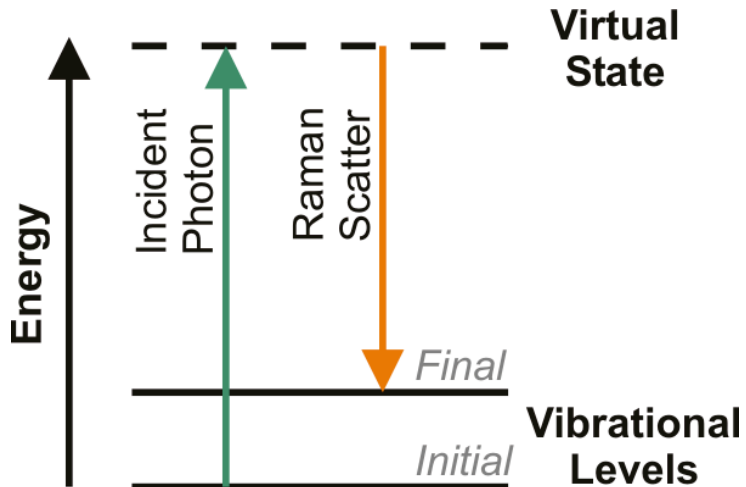

Figure 2. The DORISS instrument on the ROV Ventana. The spectrometer housing and electronics housings are mounted in a drawer in the ROV toolsled (shown by arrow). The probe head is carried in front (left in the picture below) for deployment by the ROV manipulator.
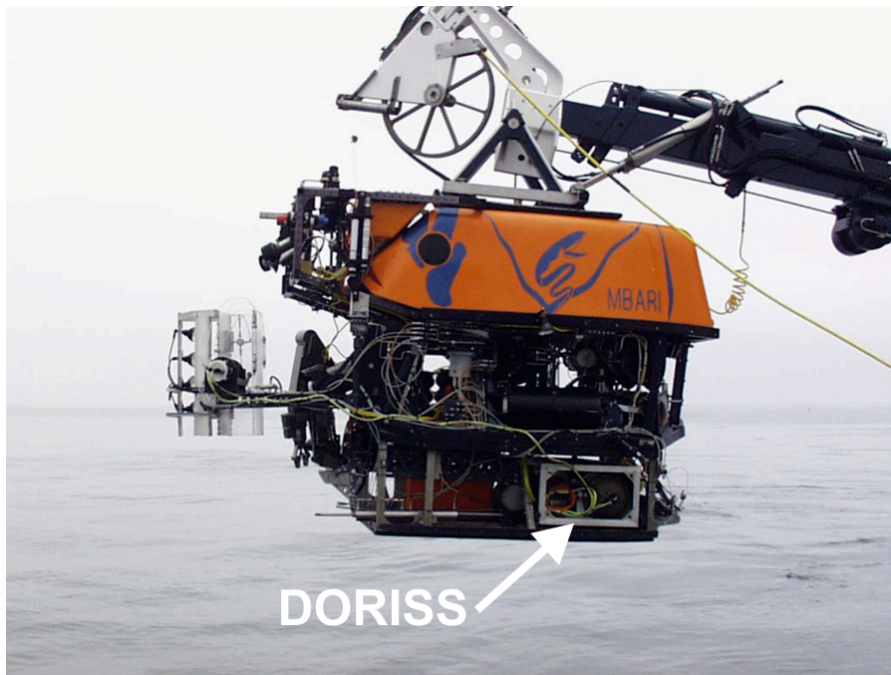
Figure 3. Phase diagram for pure CO_2 in seawater **(A)** and 50%-50% CO_2-N_2 mixture in seawater **(B)** calculated using MultiFlash 3.2 (Infochem, Inc., London). The grey regions indicate the hydrate stability zones, the dash-dotted line indicates the liquid gas boundary. The red line is a temperature profile from Monterey Bay, and the X indicates the experimental conditions of our deployments.
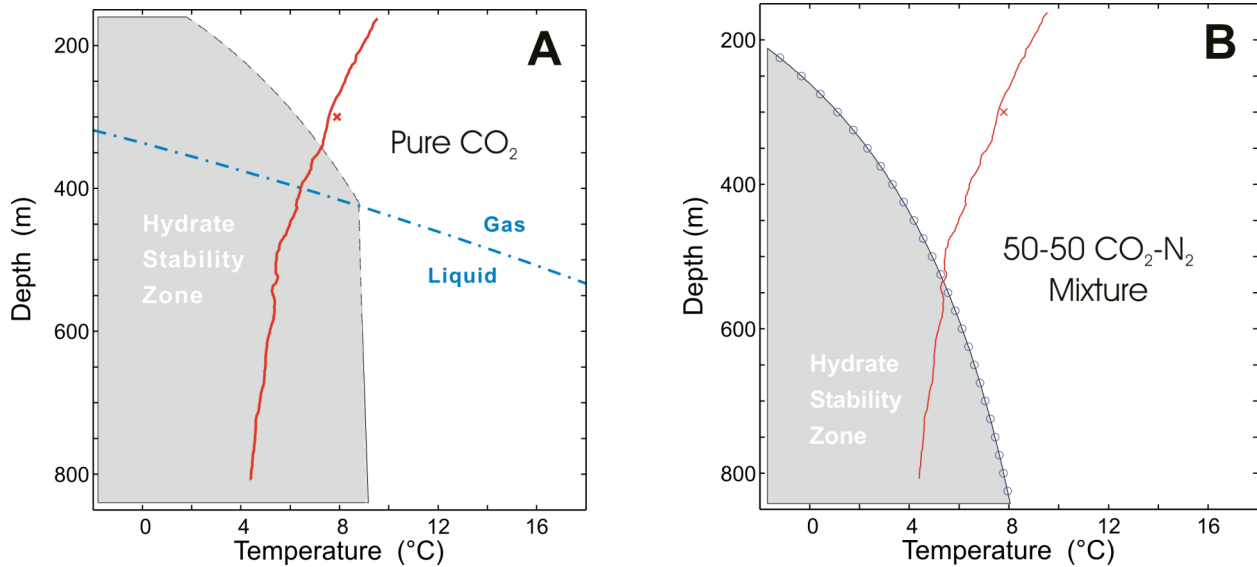
Figure 4. A video frame grab showing the DORISS probe tip penetrating the open-bottomed gas cube (10 x 10 x 10 cm). The ports at the top of the cube are used to fill and vent the cube. (From Brewer et al., 2004)
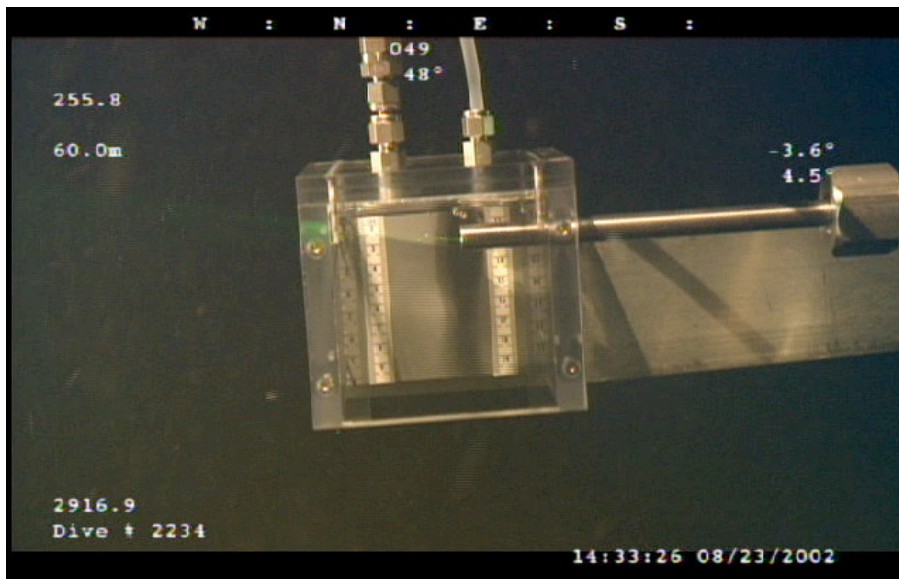
Figure 5. a) A frame grab showing the DORISS probe tip with gas funnel and gas dispensing tube. **b)** A cross-section of the experimental set up.
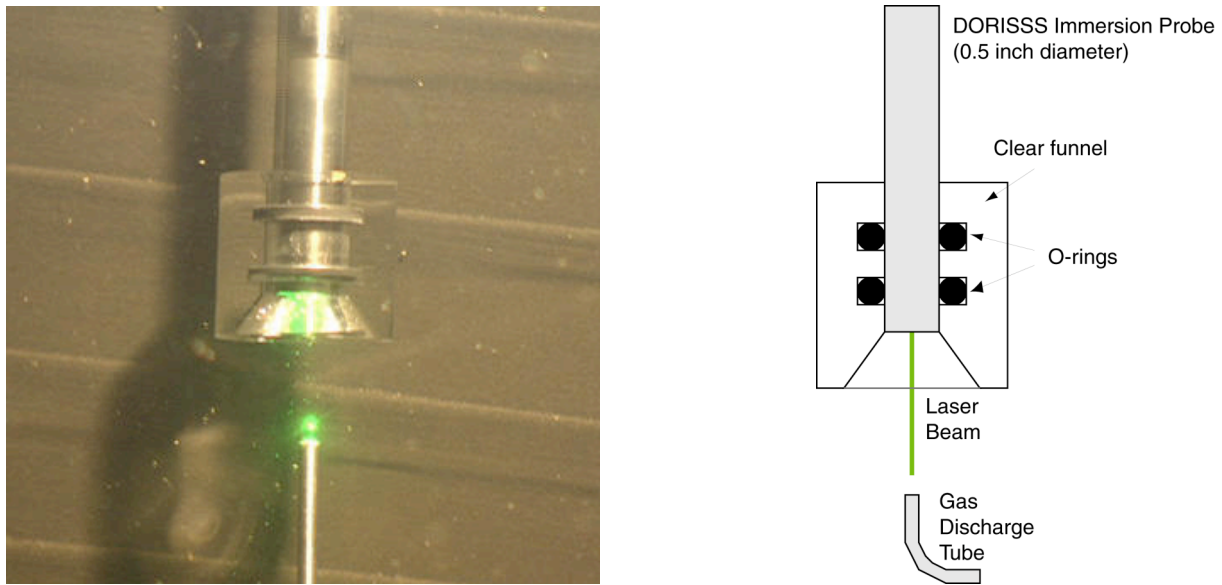
Figure 6. Raman spectra of 50%-50% CO_2-N_2 gas mixture in gas cube during August 2002 dives. The diamond reference peak is at 1332 Δcm^{-1}. The two CO_2 peaks are at 1285 Δcm^{-1} (bending mode) and 1388 Δcm^{-1} (stretching mode). The N_2 peak is at 2332 Δcm^{-1}. The drop out at ~1900 Δcm^{-1} is due to a flaw on the CCD chip.
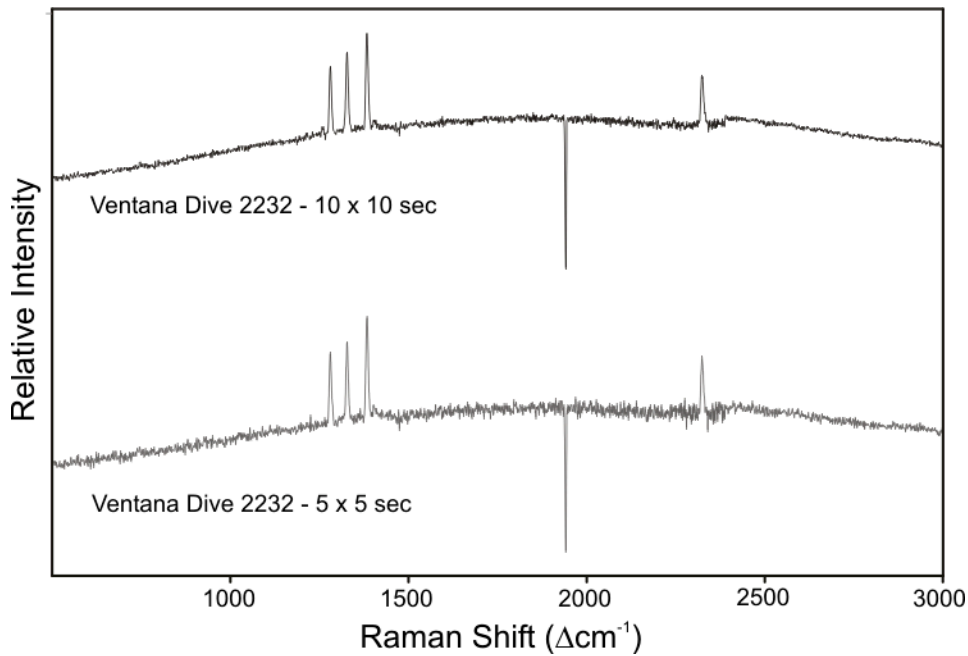
Figure 7. Peak area ratios over time from the August 2002 gas cube experiment. Data points are plotted at the midpoint of the accumulation time.
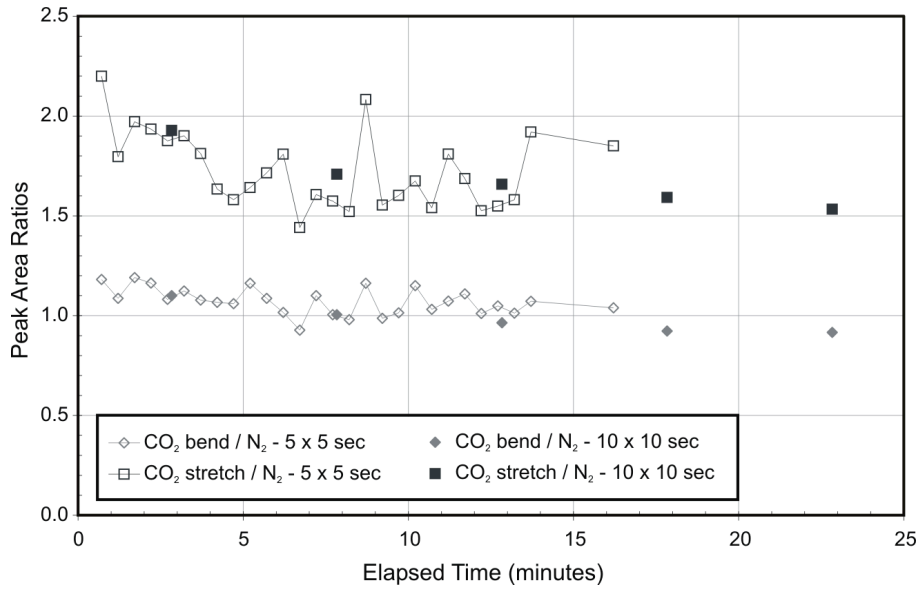

Figure 8. Raman spectra of CO_2 over time. Each spectrum is an average of fifteen 15-second exposures (3.75 minute average). The diamond reference peak is at 1332 Δcm^{-1}. The two CO_2 peaks are at 1285 Δcm^{-1} and 1388 Δcm^{-1} and decrease over time as CO_2 is dissolved into seawater. The N_2 peak is at 2332 Δcm^{-1} and is not shown in this segment of the spectra.
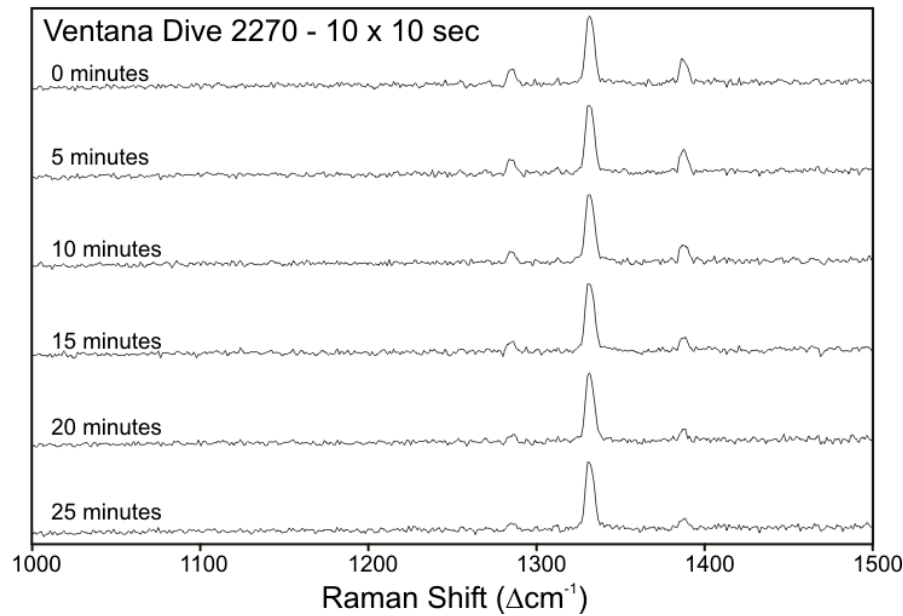
Figure 9. Peak area ratios over time for the October 2002 gas funnel experiments. Spectra from experiment 1 are averages of ten 10-second exposures (1.67 minute averages). Spectra from experiment 2 are averages of fifteen 15-second exposures (3.75 minute averages). The decrease in the ratios of the peak areas of the CO_2 bands to N_2 band can be fit by an exponential curve. Data points are plotted at the midpoint of the accumulation time.
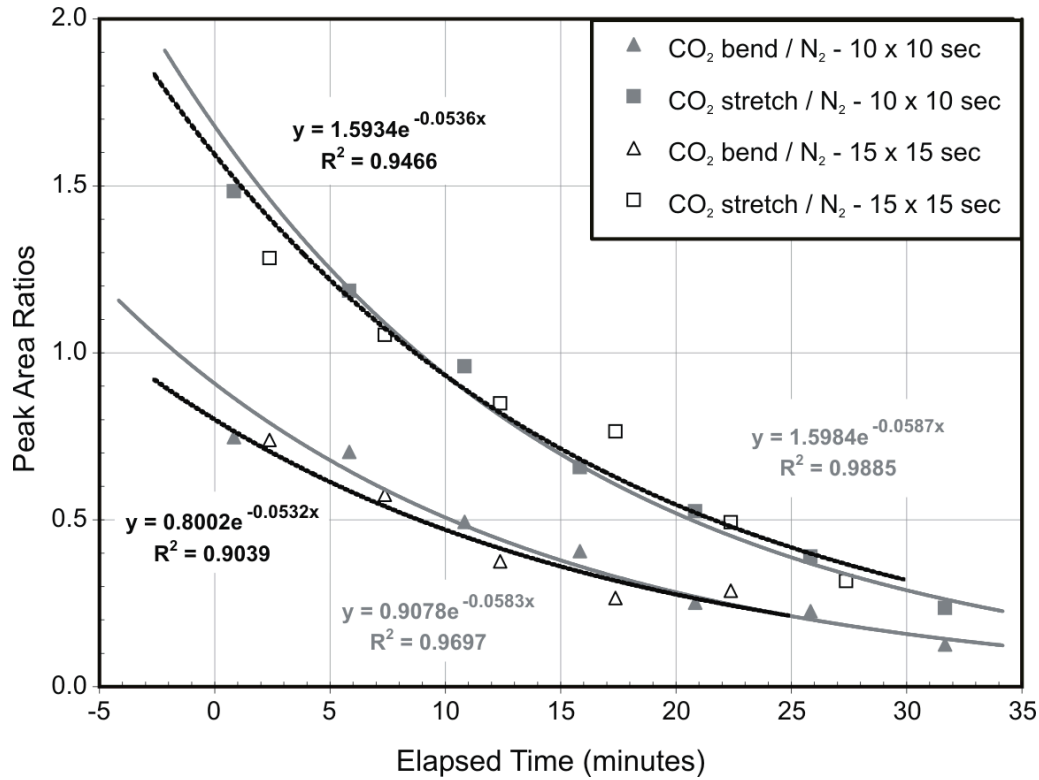
Figure 10. Observed and calculated CO_2 mole fraction from August and October deployments. The symbols indicate the observed values, the lines indicate the mole fraction calculated using the gas flux equation.